actuators

MDPI

Review

Model-Free Closed-Loop Control of Flow Past a Bluff Body: Methods, Applications, and Emerging Trends

Feng Ren [1], Xin Wen [2,*] and Hui Tang [3]

[1] School of Marine Science and Technology, Northwestern Polytechnical University, Xi'an 710072, China; renfeng@nwpu.edu.cn
[2] School of Mechanical Engineering, Shanghai Jiaotong University, Shanghai 200241, China
[3] Department of Mechanical Engineering, The Hong Kong Polytechnic University, Hong Kong, China; h.tang@polyu.edu.hk
* Correspondence: wenxin84@sjtu.edu.cn

Abstract: Flow past one or multiple bluff bodies is almost ubiquitous in nature and industrial applications, and its rich underlying physics has made it one of the most typical problems in fluid mechanics and related disciplines. The search for ways to control such problems has attracted extensive attention from both the scientific and engineering fields, as this could potentially bring about benefits such as reduced drag, mitigated noise, suppressed vibration, and enhanced heat transfer. Flow control can be generally categorized into passive and active approaches, depending on whether there is an external energy input to the flow system. Active control is further divided into open-loop approaches and closed-loop approaches, depending on whether the controller depends on feedback signals extracted from the flow system. Unlike in many other applications of passive flow control and open-loop active flow control, theoretically advantageous closed-loop controls are quite rare in this area, due to the complicated features of flow systems. In this article, we review the recent progress in and future perspectives of flow past a single or multiple bluff bodies using model-free closed-loop control so as to outline the state-of-the-art research, determine the physical rationale, and point to some future research directions in this field.

Keywords: active flow control; flow past a bluff body; machine learning

Citation: Ren, F.; Wen, X.; Tang, H. Model-Free Closed-Loop Control of Flow Past a Bluff Body: Methods, Applications, and Emerging Trends. *Actuators* **2024**, *13*, 488. https://doi.org/10.3390/act13120488

Academic Editor: Luigi de Luca

Received: 30 September 2024
Revised: 16 November 2024
Accepted: 27 November 2024
Published: 29 November 2024

1. Background

Flow past a single or multiple bluff bodies is among the most typical flow types of fluid mechanics and is almost ubiquitous in nature and engineering applications [1,2]. In general, bluff bodies produce a stronger separated flow, have a broader wake with low pressure and complicated vortical structures, and have higher drag compared with streamlined bodies. Extensive studies have been carried out, using theoretical, computational, and experimental approaches to explore the very rich physics of such flows, including flow transition, flow instability, flow separation, and diverse vortical structures, as well as to provide engineering solutions [1–4]. Taking the flow past a finite-length circular cylinder with one free end and one fixed end as an example, as shown in Figure 1, very complicated flow features can be observed, such as the horseshoe vortex that appears in proximity to the fixed end, tip vortices, shear layers, an alternately shedding Kármán vortex street, and time-mean vortices [5,6]. These flow features exert complicated forces on the bluff body, which play a crucial role in engineering applications. For instance, in the case of an underwater vehicle, reducing hydrodynamic drag not only saves energy but also improves cruising speed and range [7,8].

In addition to these pure flow systems, flow past a bluff body is also accompanied by flow-induced vibrations [9–12], flow-induced noise [13–15], heat transfer [16–18], etc., making the problem more complicated and challenging. For example, vortex-induced

vibration (VIV) is one of the most typical flow-induced vibrations that occurs when asymmetrical vortex pairs shed from a bluff body that is immersed in a uniform flow and is elastically mounted [9,11]. For different combinations of vibration amplitude and wavelength, the phase diagram (Figure 2) shows diverse wake patterns, where vortex shedding and structural motion are synchronized; these are categorized as the "mS + nP" mode. In this mode, during one vibration cycle, m single vortices and n vortex pairs are shed from the vibrating body and convect downstream [9]. In many engineering scenarios, VIV and other flow-induced vibrations are often unwanted, as they can induce mechanical fatigue or even structural damage [12,19]. Conversely, the mechanical energy that is generated can also be harnessed and exploited as green energy.

The noise generation and radiation accompanied by flow past a bluff body are also a key issue [13,15,20]. As reviewed and summarized by [13], fluctuations at the wall, viscous shear stresses at the wall, and turbulent velocity fluctuations are identified as the apparent sources of boundary-layer noise, which are closely related to the near wake. Figure 3 demonstrates the far-field dilatation of flow past a circular cylinder at $Re = 3900$ and $Ma = 0.4$, as well as the near-field wake [20]. It is straightforward to note that sound pressure waves are closely related to vortex shedding. In laminar cases, noise is primarily generated by vortex formation and shedding, where a negative pressure pulse is produced on one side of the cylinder surface from which a vortex is shed, while a positive pressure pulse is produced on the opposite side [21]. In turbulent cases, the mechanism becomes more complex, involving the effects of turbulent fluctuations [15,20]. The generation and propagation of noise play a significant role in the field of aeronautics, where environmental noise is a key factor influencing passengers' experience [15]. Flow-induced noise is particularly important for underwater vehicles, as it reduces the signal-to-noise ratio of communication and navigation devices that primarily rely on sound, thereby increasing the likelihood of detection.

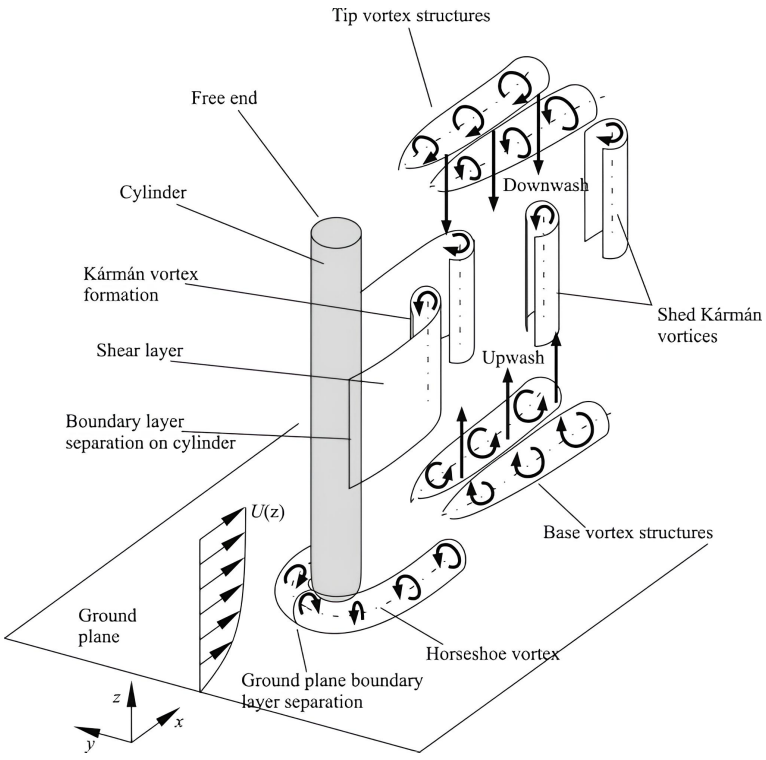

Figure 1. Schematics of flow features past a circular cylinder with one free end and the other end mounted on the wall. This figure is reproduced from the work of Sumner [5], with permission.

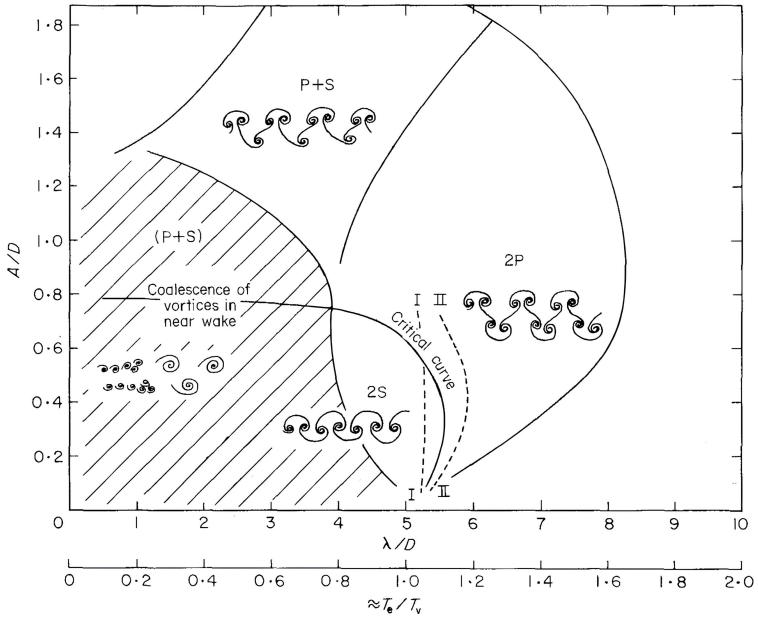

Figure 2. Map of vortex synchronization patterns of vortex-induced lateral (cross-flow) vibrations of a circular cylinder in a uniform stream. This figure is reproduced from the work of Williamson and Roshko [9], with permission.

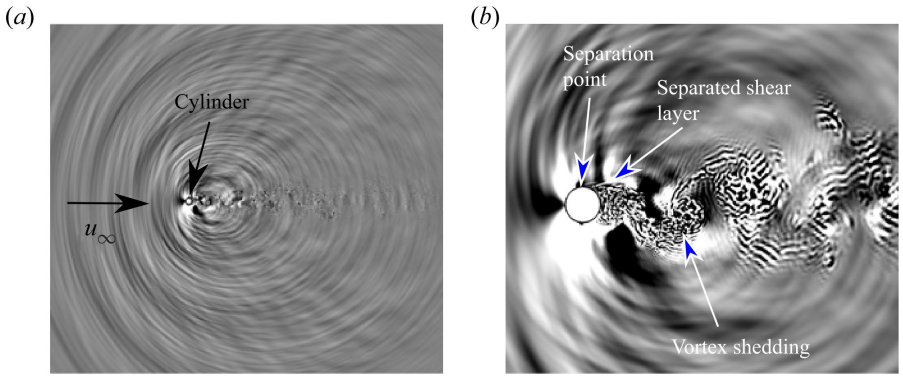

Figure 3. Instantaneous snapshots of flow past a circular cylinder in the turbulent regime: (**a**) far-field dilatation field, and (**b**) near-field wake and dilatation field. This figure is reproduced from the work of Li et al. [20], with permission.

Controlling flow past a bluff body can provide many benefits, such as drag reduction, noise mitigation, and vibration suppression [22,23]. Control strategies can generally be categorized into two main types: passive approaches and active approaches [3,12,22,24]. In recent years, as technologies such as micro-electro-mechanical systems (MEMS) have been developed [25], many advanced actuators have been invented [26], including blowing/suction jets, synthetic jets, sweeping jets, pulse jets, plasma actuators, and rotating rods. A properly chosen actuator can yield significant control effects. For example, Dong et al. [27] used the windward-suction–leeward-blowing (WSLB) actuator and successfully eliminated the Kármán vortex street. The pulse jet modulated by Abdolahipour et al. [28] can use both high and low frequencies [29], which can then control flow past an airfoil in a highly deflected flap and at high angles of attack [30], as well as controlling the vortex shedding [31]. Mirzaei et al. [32] also proved that the plasma actuator is efficient in controlling the vortex shedding. However, even with well-designed and manufactured actuators, it is often challenging to exert the precise amount of forcing needed to mediate the flow dynamics and achieve optimal performance [26].

Closed-loop flow control exerts a certain amount of energy on the flow system in a self-adaptive manner, according to the feedback signals sampled from the dynamically varying flow system and the adopted controller [33]. In scenarios where the flow system is linear, weakly linear, or moderately linear, a linear control design can usually be utilized [33,34], such as optimal control methods including the linear–quadratic regulator (LQR) and linear–quadratic–Gaussian (LQG) method. Researchers have also developed methods that rely on a model reduction in the flow systems [35,36], such as flow control methods based on proper orthogonal decomposition (POD), dynamic mode decomposition (DMD), resolvent analysis, etc. In contrast, there are also model-free methods of designing the controller that are independent of the mathematical modeling of the flow system, instead relying on methods such as parameter tuning or optimization or data-driven dynamic optimization. In the engineering field, flow systems always share nonlinear and high-dimensional features; for example, a turbulent flow and separation flow. Therefore, even though there are many successful examples of closed-loop flow control, designed using rigorous mathematical models, there is still an urgent demand for a general solution for closed-loop control that is effective, efficient, and robust, representing an ongoing research challenge [23,33].

It is thus worth reviewing previous studies in which researchers apply model-free closed-loop control strategies to address specific problems related to flow past a bluff body, especially the key elements involved therein, such as the control method, the control objective, the sensors, and the actuators. It would be interesting to lead readers to further consider what can one expect from closed-loop AFC, such as an excellent control performance or physical insights. It is also necessary to mention that, with the rapid development of machine learning, two quite promising ideas and effective tools, such as genetic programming (GP) and reinforcement learning (RL), were provided to guide the closed-loop AFC in a data-driven and model-free manner. These have attracted extensive attention in the field of fluid mechanics, especially from researchers working on flow control [37–40]. Reviewing the research cases and emerging trends can help to identify existing problems in this specific field and future perspectives. In the remaining sections of this manuscript, we categorize the current model-free closed-loop control into four types, i.e., model-free PID control, GP-based control, RL-guided control, and cluster-based control. In Table 1, some examples of model-free and closed-loop control strategies are summarized, including their methods, objectives, and the sensors and actuators they utilize.

Table 1. An overview of the methods and typical applications of closed-loop control of flow past a bluff body.

Method	Objective	Sensor	Actuation	Reference
PID control	Stabilize wake	Transverse velocity	Synthetic jets	Park et al. [41]
	Reduce vortex strength and suppress vibration	Velocity and vibration displacement	Piezoelectric ceramic actuators	Zhang et al. [42]
	Mitigate lift fluctuations	Lift	Self-rotation	Lu et al. [43]
	Reduce noise	Lift	Self-rotation	Du and Sun [44]
	Stabilize wake	Spanwise-averaged velocity	Blowing/suction jets	Yun and Lee [45]
	Suppress vibration	Transverse velocity	WSLB jets	Wang et al. [46]
	Mediate vibration	Vibration displacement/velocity	Self-rotation	Vicente-Ludlam et al. [47]
	Suppress vibration	Vibration velocity	Damping force	Song et al. [48]
	Suppress vibration	Lift	Self-rotation	Hasheminejad et al. [49]
	Suppress vibration	Vibration displacement	Control force	Rabiee and Esmaeili [50]

Table 1. *Cont.*

Method	Objective	Sensor	Actuation	Reference
GP-based control	Mitigate separation	Skin friction	Active vortex generator	Debien et al. [51]
	Reduce drag	Wall pressure	Pulsed jets	Li et al. [52]
	Stabilize wake and reduce drag	velocity	Self-rotation	Raibaudo et al. [53]
	Stabilize wake and reduce drag	Velocity	Self-rotation	Raibaudo and Martinuzzi [54]
	Suppress vibration	Vibration displacement	Blowing/suction jets	Ren et al. [55]
	Reduce drag	Velocity	Blowing/suction jets	Castellanos et al. [56]
RL-guided control	Reduce drag	Velocity array	Blowing/suction jets	Rabault et al. [57]
	Reduce drag	Velocity array	Blowing/suction jets	Ren et al. [58]
	Reduce drag	Velocity array	Blowing/suction jets	Paris et al. [59]
	Suppress vortex shedding	Velocity array	Blowing/suction jets	Li and Zhang [60]
	Reduce drag	Velocity array	Blowing/suction jets	Varela et al. [61]
	Mitigate lift	Velocity array	Self-rotation	Zhao et al. [62]
	Reduce drag	Wall pressure	Blowing/suction jets	Wang et al. [63]
	Mitigate lift	Velocity array	Self-rotation	Ren et al. [64]
	Reduce drag	Wall-pressure	Blowing/suction jets	Chen et al. [65]
	Achieve hydrodynamic stealth	Velocity array	WSLB jets	Ren et al. [66]
	Reduce drag	Force	Rotary rod	Fan et al. [67]
	Reduce drag	Force	Rotary rod	Wang et al. [68]
	Suppress vibration	Velocity array	Blowing/suction jets	Zheng et al. [69]
	Suppress vibration	Velocity array	Self-rotation	Ren [70]
	Reduce vibration	Velocity array	Blowing/suction jets	Chen et al. [71]
	Suppress vibration	Sensorymotor cues	Self-rotation	Ren et al. [72]
	Enhance vibration	Velocity array	Blowing/suction jets	Mei et al. [73]
	Enhance heat transfer	Sensorymotor cues	Blowing/suction jets	Ren et al. [74]
	Suppress vibration	Vibration displacement and velocity	Blowing/suction jets	Zheng et al. [75]
	Reduce drag	Velocity	Blowing/suction jets	Castellanos et al. [56]
Cluster-based control	Control flow separation	Force	Reduce power consumption	Nair et al. [76]
	Reduce drag	Velocity field	Self-rotation	Wang et al. [77]

2. Model-Free PID Control

In classical control theory, controllers are typically designed based on linear assumptions. The AFC also follows this principle [34]. PID control is perhaps the most classical control approach and is extensively utilized in engineering fields. In the closed-loop AFC of flow systems, the interpretation of PID control differs slightly from that in classical control theory. In our view, PID control is primarily considered a model-free approach. By tuning the control parameters, certain control performance can be achieved.

The PID control has been proven to be effective and efficient in controlling flow past a bluff body. For example, Park et al. [41] applied a proportional control strategy to stabilize the Kármán vortex street at Reynolds numbers lower than 100, where a pair of synthetic jets is deployed near the separation point, and the transverse velocity at a selected downstream position is used to provide feedback signals. With this relatively simple strategy, vortex shedding is completely suppressed at $Re = 60$. Zhang et al. [42] performed an experimental study of PID control for the vortex shedding and vibration of an elastically supported square cylinder in the turbulent flow regime. They investigated different feedback signals, including turbulent velocity, structural vibration displacement, and combinations thereof, showing that feedback from both flow and structural vibrations can remarkably reduce vortex strength as well as vibration amplitude. Lu et al. [43] applied proportional control to suppress the transverse lift of a circular cylinder at low Reynolds numbers, where

the rotational velocity of the cylinder is proportional to the instantaneous lift coefficient exerted on the cylinder. It was found that the control performance is closely related to the proportional control parameters, and the optimal control parameters vary with the Reynolds number. Using the same method but different flow conditions and a different control objective, Du and Sun [44] applied proportional control to reduce noise in a circular cylinder at $Re = 1000$, showing that the noise generated by the cylinder can be reduced by 10 dB due to the suppression of vortex shedding. Figure 4 shows the instantaneous vortical structures with and without control. Based on Curle's acoustic analogy [78], the noise generated by the solid wall is primarily attributed to force fluctuations. Thus, the objectives of lift suppression and noise reduction would lead to similar physical attributes. Yun and Lee [45] applied proportional control to turbulent flow over a circular cylinder with a similar blowing/suction jet configuration to that in Ref. [41], while the feedback transverse velocity was averaged along the spanwise direction.

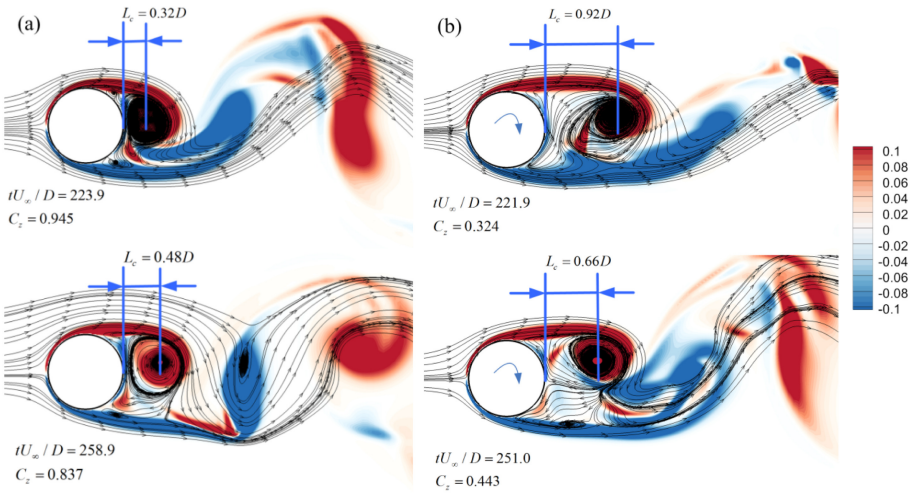

Figure 4. Instantaneous vortical structures of flow past a circular cylinder at $Re = 1000$: (**a**) uncontrolled case, and (**b**) a case with proportional control. This figure is reproduced from the work of Du and Sun [44], with permission.

Controlling the VIV using the PID controller is of great interest. Wang et al. [46] carried out a systematic parametric study on the effects of proportional and PI control, where two groups of WSLB actuators are used to mediate the flow dynamics near the cylinder, and a transverse velocity feedback signal in the near wake is utilized. Within certain control parameter ranges, VIV can be effectively suppressed. Vicente-Ludlam et al. [47] studied rotary control to manage the VIV of a circular cylinder in an experimental environment within a Reynolds number range of 1500 to 10,000. The rotation rate was made proportional to either the cylinder's vibration displacement or its vibration velocity, similar to the concepts of proportional control and proportional–derivative control. Both control laws resulted in reduced or enhanced oscillations. A recent study by Song et al. [48] applied PID control to suppress VIV with two degrees of freedom and demonstrated that PI or PID control can significantly reduce the vibration range in both the streamwise and transverse directions by 68.4% to 97.1%.

In PID control, determining the control variables is usually a difficult task, especially when the flow system involves turbulence or fluid–structure interaction (FSI), or when the controller has multiple inputs and/or multiple outputs (MIMO). In the field of control theory, there are also problems when the system to be controlled is regarded as a black box whose transfer function cannot be directly obtained. Feasible solutions include adaptive control methods, fuzzy control, sliding mode control, and others. Researchers working on closed-loop AFC have also used this idea. For example, Hasheminejad et al. [49] applied fuzzy proportional control for the VIV of a circular cylinder under laminar flow conditions. Three different proportional controllers were studied, all of which outperformed

the representative open-loop control with the prescribed rotational oscillations. Rabiee and Esmaeili [50] further applied fuzzy PID control to control the flow-induced vibrations of two circular cylinders in tandem configuration with the aid of a fuzzy logic system. A schematic diagram of the coupling framework of the controller and the numerical environment is demonstrated in Figure 5, where the desired control force is determined using the feedback signals from vibration displacement.

Because the flow system is nonlinear in nature, while PID control theory is developed based on linear approximations, the effectiveness and robustness of PID control may be limited to flow systems with weak nonlinearity, primarily in the laminar regime. In turbulent conditions, special treatments must be implemented, such as using the spanwise-averaged sensing signal Yun and Lee [45]. Due to the gap between linear control theory and nonlinear flow systems, PID control must be systematically studied before being applied in practical scenarios.

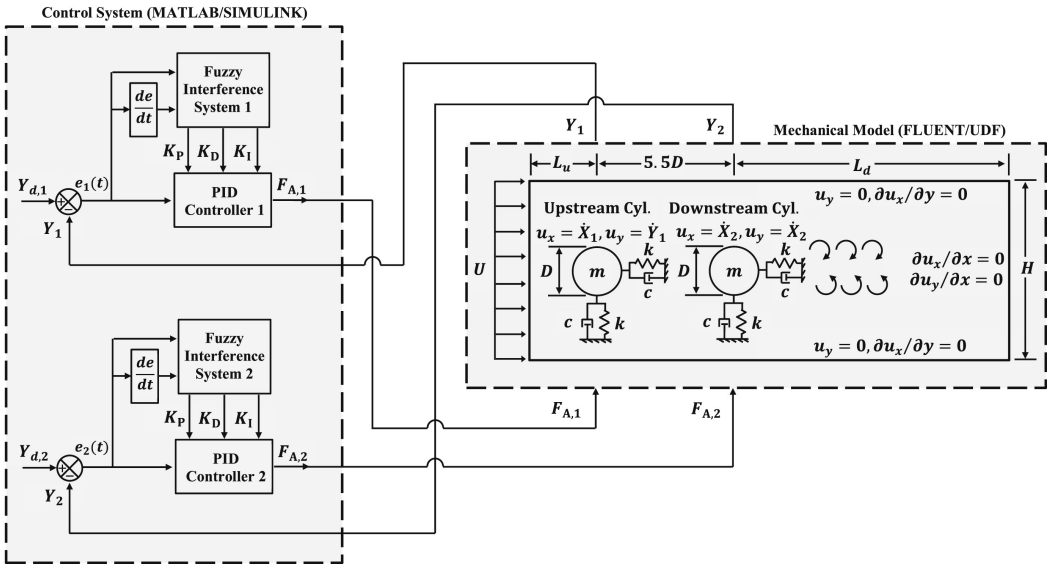

Figure 5. Schematics of the coupling framework between the fuzzy PID controllers and the CFD model. This figure is reproduced from the work of Rabiee and Esmaeili [50], with permission.

3. Genetic Programming-Based Control

Compared to the aforementioned PID control, control methods that are independent of prior knowledge of the flow system are attractive, as they can provide a general solution for closed-loop flow control, especially when addressing the challenging task of modeling complicated flows and determining appropriate parameters to adjust control performance. Among these model-free methods, machine learning has attracted increasing attention from the flow control community. Most machine learning approaches share data-driven features, making their application in problems in fluid mechanics feasible due to the large amount of data available from experiments and numerical simulations. The applications of machine learning in fluid mechanics were reviewed previously [39,79–81].

In this section, GP-based control is reviewed. GP stems from the genetic algorithm (GA), which is usually used to optimize one or multiple values. In GP, symbolic expressions are involved in the evolution process, with the aid of the locator/identifier separation protocol (LISP) language. Because these symbolic expressions can naturally function as explicit control laws, GP can be used to generate and select the optimal control law, similarly to the way in which optimal parameters are determined by the GA. Both GP and GA share an evolutionary algorithm. Here, a group of individuals participate in the natural selection, and only a few individuals are selected to generate the next generation through crossover, replication, mutation, etc. Figure 6 shows the mutation of an individual and the crossover between two individuals Gautier et al. [82].

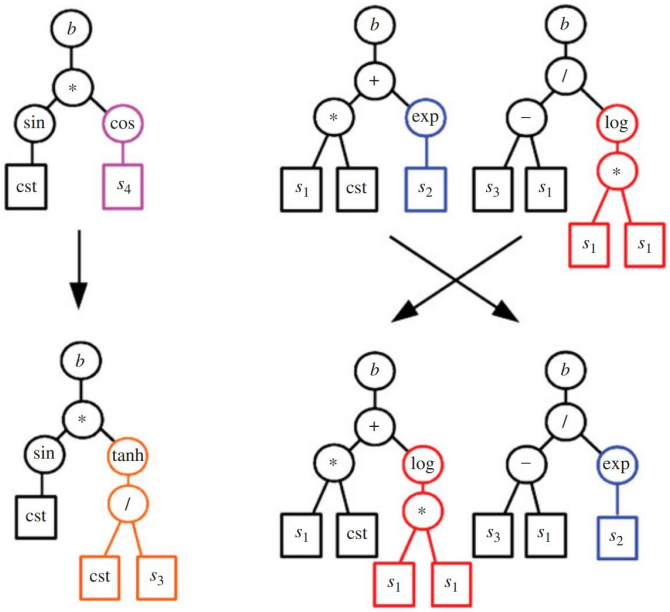

Figure 6. An example of mutation of an individual (**left subfigure**) and an example of crossover between two individuals (**right subfigure**). This figure is reproduced from the work of Gautier et al. [82], with permission.

Gautier et al. [82] were perhaps the first to apply GP to closed-loop AFC, where the backward-facing step is controlled by blowing/suction jets deployed near the step corner. Using a similar method and idea as those of Gautier et al. [82], Debien et al. [51] conducted a closed-loop control of flow over a sharp edge ramp, targeting separation mitigation and early re-attachment. Active vortex generators were used to mediate the flow, and downstream skin-friction sensors provided feedback information. Comparisons with the open-loop control experiments show that the open-loop system utilizes the lock-on effect, while the GP-based control accelerates shear layer growth with a lower energy. Li et al. [52] carried out a closed-loop control of flow past the blunt-edged Ahmed car model based on linear GP. Multiple pulsed jets at all trailing edges were utilized as actuators, which were also combined with a deflection surface to exploit the Coanda effect. A group of wall pressure sensors deployed at the rear side was then used to provide feedback signals. In an unsupervised manner, the linear GP-based control achieved an approximately 22% drag reduction rate.

Raibaudo et al. [53] performed experiments in which linear GP was utilized to stabilize the wake of a fluidic pinball and reduce drag. The velocities from three hot-wire sensors were used to provide feedback signals and the constant rotational velocities of three cylinders were used to mediate the flow dynamics. The results show that the GP-based strategies reveal unanticipated solutions or parameter relationships. To account for the effects of unsteady actuation, Raibaudo and Martinuzzi [54] conducted further experimental studies in which each cylinder of the fluidic pinball was controlled independently and could vary periodically. The results indicate that the GP-based control was more efficient than traditional methods at optimizing within a large parametric space and was also more robust than open-loop control. Ren et al. [55] used the GP to actively control the VIV of a circular cylinder under lock-in conditions. Figure 7 shows the schematics of the GP-based control, where the upper module represents the dynamic FSI system and the lower module represents the GP agent. The converged control law suppresses the VIV amplitude by 94.2% and achieved a 21.4% better overall performance than the best proportional control at a Reynolds number of $Re = 100$. In robustness tests across a Reynolds number range of 100 to 400, the GP-based control law remains highly effective, while the proportional control, which is suitable for $Re = 100$, fails the test.

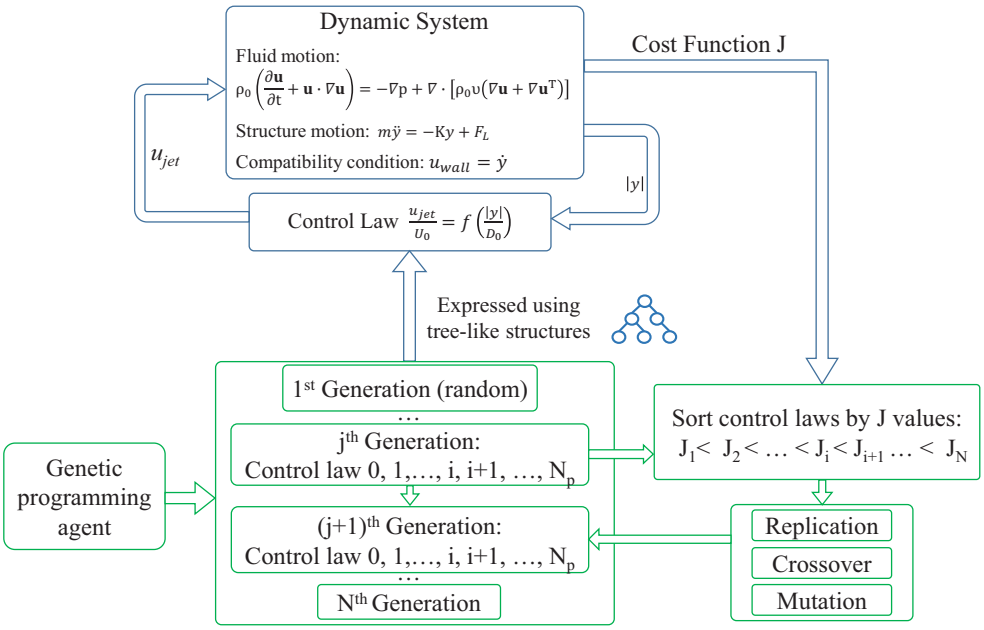

Figure 7. Framework of the GP-based control for vortex induced vibration control in the numerical environment based on the LBM. This figure is reproduced from the work of Ren et al. [55], with permission.

In a numerical environment, the evolutionary algorithm typically utilizes hundreds or thousands of individuals until the control performance converges. Therefore, it is crucial to employ a computationally efficient simulation tool. For example, in the aforementioned study by Ren et al. [55], a lattice Boltzmann solver accelerated on a graphics processing unit device [83,84] is used, allowing for a single case initialized with a fully developed flow field to be completed in 20 min or less.

In an experimental environment, an individual trial can usually be completed within just a few minutes, which is more advantageous than the numerical approach. The hardware costs in terms of real-time signal recording and a fast actuation response, as well as the uncertainties during the experimental study, are other crucial issues that need to be addressed.

4. Reinforcement Learning-Guided Control

RL is an important branch of machine learning. In RL, an agent interacts with a dynamic environment, perceives the environment's state, and learns actions through trial and error in order to gain a high reward [85]. RL is usually combined with deep neural networks for decision-making and performance evaluation, and is then referred to as DRL. RL is applied to environment-interactive tasks such as the game of Go [86], where the RL agent learns from scratch rather than relying on the human knowledge that AlphaGo adopts [87]. RL has also been applied to train a simplified glider model to exploit upward plumes in sunny weather to soar higher [88]. Verma et al. [89] applied RL to train a fish to swim efficiently. These successes have inspired researchers in the field of fluid mechanics to tackle the closed-loop AFC problem. Thorough reviews of the use of RL in AFC can be found in the previous literature [79–81,90,91].

Unlike conventional approaches to constructing a controller, which rely heavily on prior knowledge of the system, the RL agent does not have any prior knowledge of fluid dynamics, and is thus regarded as a model-free approach. Diverse RL algorithms and their associated framework can be applied to AFC [92]. Herein, we use the popular proximal policy optimization (PPO) [93] as an example. In the interactive framework, effective control strategies are learned through interactions between the RL agent and the flow-related environment. Initially, the RL agent interacts with the environment using randomized

actions. Through trial and error, it learns how to exert a specific action when the system is in a particular state. Simultaneously, it learns how to predict the long-term reward based on this state information. The state of the environment can be represented by velocity probes, wall normal and/or shear stresses, sensory–motor cues in flow-induced vibration problems, etc. The model's actions can include adjustable jet velocity, rotary motion, and body force. During the training, the reward is evaluated and fed back to the RL agent, providing a baseline for the agent to learn how to assess control performance and encouraging it to achieve a greater reward. Figure 8 shows the schematics of RL-guided AFC for enhancing thermal convection from an elastically mounted circular cylinder, which involves the basic interactive relationship between the RL agent and the flow environment [74]. In this setup, the agent receives the state of the flow system, determines the action, and judges whether the current action earns a good reward. The control strategy is updated after sampling a state–action–reward chain within one episode.

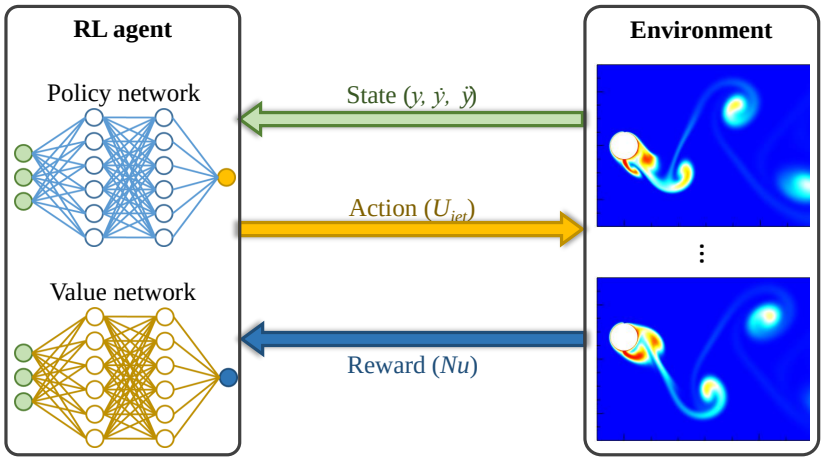

Figure 8. Schematics of RL-guided AFC for enhancing the thermal convection of a circular cylinder undergoing VIV. This figure is reproduced from the work of [74].

Before being applied to AFC, RL is utilized to maneuver the motion of a gliding bird to achieve higher altitudes by taking advantage of rising plumes in sunny weather [88], as well as to guide fish-swimming to exploit wake vortices and save energy [89]. In the more straightforward applications of RL in AFC, Rabault et al. [57] were perhaps the first to apply RL to obtain a closed-loop AFC strategy for drag reduction in a circular cylinder confined to a channel. In this pioneering work, two synthetic jet actuators were deployed at the top and bottom stagnation points of the cylinder and operated in a one-blowing–one-suction mode. A group of sensors was placed both around the cylinder and in the wake. The final converged strategy achieves an approximately 8% drag reduction rate at a fixed Reynolds number of 100. Ren et al. [58] extended intelligent flow control in laminar situations to weakly turbulent conditions where the Reynolds number was 1000, and the baseline flow exhibited many chaotic features. With a similar control setup to that of Rabault et al. [57], an approximately 30% drag reduction rate was achieved, along with mitigated lift fluctuations. Moreover, through a sensitivity analysis, it was noted that only a subset of the 151 velocity sensors play key roles in the converged control strategy. This finding provides a simple yet promising solution for reducing the number of sensors and optimizing the sensor layout. Paris et al. [59] applied RL to reduce the drag of a cylinder under laminar conditions while focusing on the efficiency and robustness of the identified control strategy, and proposed an improved RL algorithm to optimize the sensor layout. The obtained control strategy was shown to be robust within a Reynolds number range of $[100, 216]$ and to measurement noise. Li and Zhang [60] applied RL to suppress vortex shedding from a wall-confined cylinder by embedding the physical information of the flow into the RL-based control. Global linear stability and sensitivity analyses based on the time-mean flow and steady flow were conducted across a range of blockage ratios and Reynolds numbers, which were then used

to design RL-based control policies that can outperform the gradient-based optimization method. Varela et al. [61] explored the use of an intelligent AFC of a circular cylinder over a wide range of Reynolds numbers and identified different control strategies using DRL as the Reynolds number increased. For $Re \leq 1000$, the control strategy was mainly based on classical opposition control relative to wake oscillation. For $Re = 2000$, the agent applied a high-frequency actuation that energized the boundary layers and the separation zone, further modulating flow separation and reducing drag in a manner similar to that of the drag crisis. Zhao et al. [62] used DRL-guided AFC to mitigate the lift fluctuations in a circular cylinder placed in the wake of an upstream, equal-size cylinder in a tandem configuration. Through an analysis of the flow structures, it was revealed that the learned policy accelerates the shear layer development in the rear cylinder, subsequently adjusting its interaction with the wake of the front cylinder. Wang et al. [63] proposed a self-learning algorithm for reducing drag and mitigating lift fluctuations in a cylinder based on DRL. By transforming the sensor signals into dynamic features that can predict future flow states, the performance of RL-guided control can be significantly improved. Ren et al. [64] carried out intelligent controls aiming to mitigate the fluctuations in a single circular cylinder and a wake-interfered circular cylinder, respectively. With six feedback velocity signals placed near the wake, a lift mitigation rate of larger than 90% was achieved for both scenarios. In addition to the velocity sensors, many researchers used this method to study feedback; Chen et al. [65] used wall pressure, monitored at the surface of a circular cylinder, and achieved both drag reduction and lift mitigation for $Re \in [100, 400]$.

The RL can also be used to realize unconventional AFC objectives. Ren et al. [66] proposed the concept of hydrodynamic stealth and provided an RL-based solution. In this concept, five pairs of WSLB jets are used to eliminate the velocity deficit, while a velocity rake consisting of 33 velocity sensors placed in the near wake provides feedback signals. Figure 9 shows the learning process, which consists of 1000 episodes. As the learning proceeds, the wake signature gradually vanishes. Ultimately, the wake signature disappears, and the downstream velocity profile at a distance of two diameters from the cylinder becomes almost identical to the clean stream in front of the cylinder.

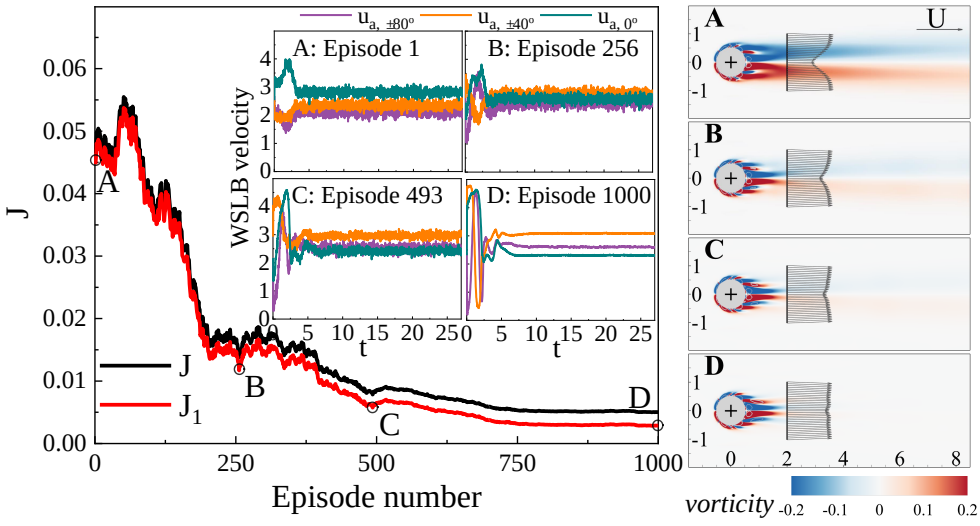

Figure 9. Training process of the reinforcement learning guided closed-loop control to achieve hydrodynamic stealth. Four subplots denote the instantaneous wake patterns and measured velocity profiles at four selected stages. This figure is reproduced from the work of Ren et al. [66], with permission.

The applications of RL-based AFC in complicated environments, such as turbulent flows, have attracted considerable attention. Fan et al. [67] demonstrated the effectiveness of RL in bluff body control through experiments, aiming to maximize power gain efficiency by adjusting the rotational speed of two small cylinders located parallel to and downstream of

the main cylinder. By properly defining rewards and designing noise reduction techniques, the RL agent discovered a control strategy that is comparable to the optimal strategy found through systematically planned control experiments. Wang et al. [68] considered the canonical flow past a circular cylinder, whose wake is controlled by two small rotating cylinders. The trained DRL agent, developed from inexpensive simulations at low Reynolds numbers, is transferred to cases at Reynolds numbers of up to 1.4×10^5, leading to successful control strategies that are feasible for high-Re conditions.

In the aforementioned work [66], the hydrodynamic stealth in the VIV scenario is also tested, which clearly shows that the VIV is almost fully suppressed alongside an almost vanished wake signature. It is thus quite natural to apply the RL-guided AFC to control classical flow-induced vibration problems. Zheng et al. [69] applied RL to control the VIV of a circular cylinder and made comparisons with an active learning approach, where a Gaussian process regression surrogate model is used to predict the VIV amplitude, combined with a Bayesian optimization algorithm for specified control actions. The RL agent was found to be able to suppress the VIV by 82.7%, outperforming the active learning approach, which reduced the VIV amplitude by only 28.3%. Ren [70] studied VIV control using feedback signals consisting of an array of velocity sensors. The final VIV suppression rate was 89%, achieving a slightly better control performance than that shown in Ref. Zheng et al. [69] while using far fewer sensors. Chen et al. [71] used DRL-based AFC to mitigate the VIV of a square cylinder, reducing the vibration amplitude by 86%, 79%, and 96% for three jet positions deployed at the front, middle, and back sides of the square cylinder, respectively. Using a state space that consists solely of sensory–motor cues, Ren et al. [72] employed DRL-guided AFC for VIV control, highlighting the interpretability of the exploration path. It was found that different state spaces yield different trajectories, as illustrated in Figure 10. Furthermore, by analyzing the phase diagram recorded during training, three distinct stages were identified, which can be interpreted from physical perspectives.

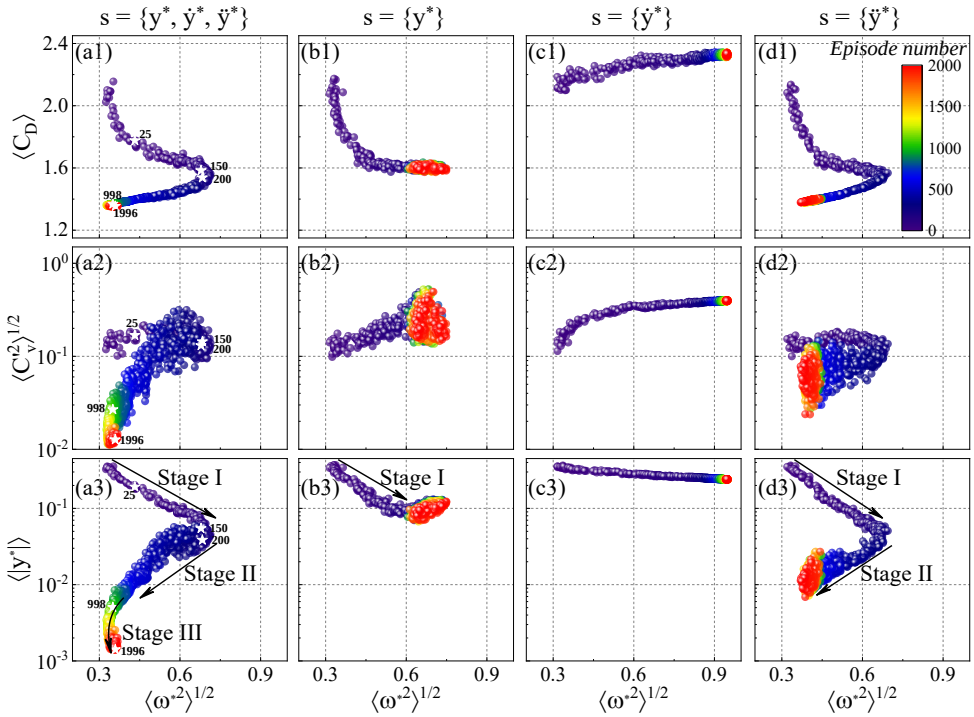

Figure 10. Trajectories of the (**a**) mean drag, (**b**) root-mean-square (RMS) of the vortex force, and (**c**) absolute value of the transverse displacement against the AFC forcing strength during training. Four training processes with different combinations of sensory–motor cues are shown in the four columns. The scattered points are colored according to the episode number. This figure is reproduced from the work of Ren et al. [72], with permission.

In contrast, increasing the VIV amplitude is sometimes advantageous; for example, Mei et al. [73] applied RL-guided jet control to enhance the energy-harnessing efficiency of a circular cylinder undergoing VIV. The jets on the cylinder were found to destabilize the vortex shedding and enhance the VIV, leading to a net energy output increase of 357.63%. Ren et al. [74] applied RL to enhance the heat transfer from a circular cylinder undergoing VIV. Unlike the typically adopted state space, which consists of high-dimensional state representations using velocity feedback signals, this study utilizes the sensory–motor cues of the cylinder, specifically the cross-flow displacement, velocity, and acceleration. The learned strategy ultimately achieved a remarkable improvement in the heat transfer rate of 76.7%.

A reliable flow environment is the basis of successful RL-guided AFC, whether numerical or experimental. The low efficiency of data acquisition and data sampling has attracted a lot of attention. Until now, most applications using numerical simulations were based on the finite element method [57] combined with the Python TensorForce package. Developing the DRL framework with open-source software [94] or commercial software [95] is also quite constructive for the community. Other approaches, such as LBM [58,66,72] or its variants [74], coupled with the Python TensorFlow library, also provide powerful solutions for RL-guided AFC due to the high-fidelity features of the LBM and its superior parallel efficiency with GPU devices. More recent studies [96,97] provide even more effective and efficient numerical tools for flow past a bluff body and are capable of simulating the flow field, structural vibrations, and acoustic field simultaneously. This is believed to provide more solutions, enabling efficient data acquisition to be achieved using numerical approaches. Rabault and Kuhnle [98] further proposed an accelerating method utilizing multiple environments to learn in a distributed configuration. Because the environments can be simulated in a parallel manner, the learning efficiency can be greatly improved. Other approaches, such as expert demonstrations that rely on a simplified mathematical modeling of the system and model optimization [75], also provide very promising directions to explore.

Comparisons of RL-based control with other existing approaches have also attracted attention. Pino et al. [99] performed a comparison of GP-based control, RL-guided control, and global optimization methods, including Bayesian optimization and Lipshitz optimization, along with an in-depth analysis. The difference in exploration versus exploitation, as well as in model capacity and required complexity, were comprehensively illustrated. Furthermore, the authors point out that the hybridization of these methods for flow control is a promising field. In the study of Castellanos et al. [56], both the DRL and the linear GP were applied to control the laminar flow past a circular cylinder, with a few velocity sensors providing feedback. Straightforward comparisons were provided using this well-designed setup, which implied that DRL is more robust with respect to its initial conditions and observation noise while linear GP is more efficient, requiring less sensor data.

Finally, with the emergence of the successful applications of RL-guided AFC in complicated flow systems and the elucidation of more rationales for these successes, it is anticipated that RL-guided control will become a general and reliable solution for the closed-loop control of flow past a bluff body and beyond.

5. Cluster-Based Control

Based on the methods from statistical mathematics, as well as a physical understanding of the flow system, other data-driven approaches are emerging, with one of the most representative being cluster-based control. Cluster-based control stems from cluster analysis, where the feature space is partitioned into groups sharing similar attributes (clusters), which correspond to coarse-grained characteristic phases in a low-dimensional (typically two-dimensional or three-dimensional) feature space [76,100]. The system dynamics are then represented as linear and probabilistic Markov chains, and transitions between clusters are considered transitions between flow states [76,100]. Active control is then established on the low-dimensional representations of the flow system in a model-free and relatively

low-cost manner. The framework of cluster-based AFC for flow past a post-stall airfoil is shown in Figure 11.

Nair et al. [76] proposed a cluster-based control strategy for the feedback control of post-stall separated flows past an NACA 0012 airfoil in the turbulent regime, utilizing a limited number of force sensor measurements to reduce power consumption during aerodynamic flight. Wang et al. [77] presented a cluster-based control strategy for model-free feedback drag reduction with multiple actuators and full-state feedback, which was demonstrated in the case of flow past a fluidic pinball using three flow regimes: symmetric periodic, asymmetric periodic, and chaotic vortex shedding. The net drag reductions for these cases amounted to 33.06%, 24.15%, and 12.23%, respectively, highlighting the distinct advantages of robust control under varying flow conditions.

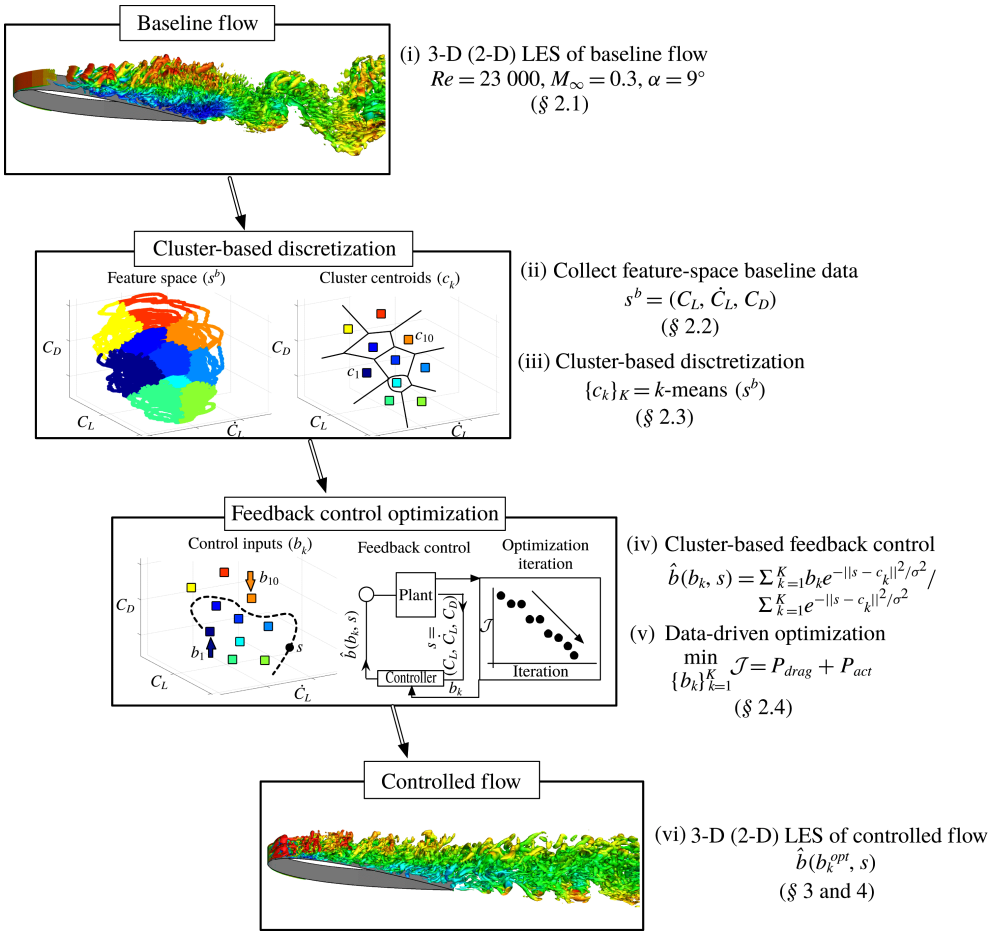

Figure 11. Overview of the cluster-based control framework. This figure is reproduced from the work of Nair et al. [76], with permission.

6. Future Prospects and Challenges

In this article, we reviewed progress in the use of model-free closed-loop control for flow past a bluff body. From the presented applications, closed-loop control is shown to be quite promising in effectively and efficiently managing flow past a bluff body. Although it has attracted attention from multiple disciplines, challenges in closed-loop active flow control also exist, such as the following:

- In numerical approaches, the problem of low-efficiency data acquisition and sampling still needs to be addressed. This area of research is quite promising given the rapid development of computational algorithms and hardware. For experimental approaches, due to the uncertainty in perturbed flows and measurement devices, the need for reliable data acquisition still needs to be addressed. Regarding these efforts,

it is quite promising to see the increase in the applications of closed-loop control in realistic scenarios.

- The effectiveness of the control performance is always the first priority. With the aid of advanced control methods, such as machine learning-based approaches, further improving effectiveness in tasks such as flow past a circular cylinder in the laminar regime is no longer challenging. However, in complicated situations involving turbulent flow, multiphysics fields, chemical reactions, etc., more efforts are essential. In our view, machine learning, especially reinforcement learning, is the most promising approach to provide a general solution to these complicated problems.
- Efficiency is a significant requirement due to the demands in the practical engineering field. Net energy savings are essential when viewing the system as a whole. For instance, it is usually not a good choice to reduce the drag of an object at the cost of increased energy consumption.
- Robustness is a special and vital topic. For the AFC, robustness involves the control responses when certain levels of perturbations are applied or when the system conditions are altered. In our view, to achieve better robustness, the process through which the final control strategy is derived should involve sufficient randomness and/or take into account a wide range of realistic perturbations.
- For data-driven, machine learning-based approaches, the interpretability of the evolution or learning path, as well as the physical rationale behind the final converged strategy, can be significant obstacles. Elucidating both issues requires knowledge of statistical mathematics, stability analyses, sensitivity analyses, resolvent analyses, etc.

Author Contributions: Conceptualization, F.R., X.W. and H.T.; investigation, F.R., X.W. and H.T.; resources, F.R.; writing—original draft preparation, F.R., X.W. and H.T.; writing—review and editing, F.R., X.W. and H.T.; visualization, F.R.; supervision, H.T.; project administration, F.R., X.W. and H.T.; funding acquisition, F.R., X.W. and H.T. All authors have read and agreed to the published version of the manuscript.

Funding: This research was funded by the National Natural Science Foundation of China (12102357), the Key Research and Development Program of Shaanxi (2023-YBGY-389), the Young Talent Fund of Xi'an Association for Science and Technology (959202413092), and the NPU Proof of Concept for Future Aerospace and Propulsion Industry (24GNYZ0001-03).

Data Availability Statement: The data used in this work are available upon request to the corresponding author.

Conflicts of Interest: The authors declare no conflicts of interest.

Abbreviations

The following abbreviations are used in this manuscript:

DMD	Dynamic mode decomposition
FSI	Fluid–structure interaction
GA	Genetic algorithm
GP	Genetic programming
GPU	Graphic processing unit
LBM	Lattice–Boltzmann method
PID	Proportional Integral and Differential
POD	Proper orthogonal decomposition
RL	Reinforcement learning
DRL	Deep reinforcement learning
WSLB	windward–suction–leeward blowing

References

1. Derakhshandeh, J.; Alam, M.M. A review of bluff body wakes. *Ocean. Eng.* **2019**, *182*, 475–488. [CrossRef]
2. Lekkala, M.R.; Latheef, M.; Jung, J.H.; Coraddu, A.; Zhu, H.; Srinil, N.; Lee, B.H.; Kim, D.K. Recent advances in understanding the flow over bluff bodies with different geometries at moderate Reynolds numbers. *Ocean. Eng.* **2022**, *261*, 111611. [CrossRef]

3. Rashidi, S.; Hayatdavoodi, M.; Esfahani, J.A. Vortex shedding suppression and wake control: A review. *Ocean. Eng.* **2016**, *126*, 57–80. [CrossRef]
4. Mondal, R.; Alam, M.M. Blockage effect on wakes of various bluff bodies: A review of confined flow. *Ocean. Eng.* **2023**, *286*, 115592. [CrossRef]
5. Sumner, D. Flow above the free end of a surface-mounted finite-height circular cylinder: A review. *J. Fluids Struct.* **2013**, *43*, 41–63. [CrossRef]
6. Zhang, D.; Cheng, L.; An, H.; Draper, S. Flow around a surface-mounted finite circular cylinder completely submerged within the bottom boundary layer. *Eur. J. Mech.-B/Fluids* **2021**, *86*, 169–197. [CrossRef]
7. Hasan, K.; Ahmad, S.; Liaf, A.F.; Karimi, M.; Ahmed, T.; Shawon, M.A.; Mekhilef, S. Oceanic Challenges to Technological Solutions: A Review of Autonomous Underwater Vehicle Path Technologies in Biomimicry, Control, Navigation, and Sensing. *IEEE Access* **2024**, *12*, 46202–46231. [CrossRef]
8. Wynn, R.B.; Huvenne, V.A.; Le Bas, T.P.; Murton, B.J.; Connelly, D.P.; Bett, B.J.; Ruhl, H.A.; Morris, K.J.; Peakall, J.; Parsons, D.R.; et al. Autonomous Underwater Vehicles (AUVs): Their past, present and future contributions to the advancement of marine geoscience. *Mar. Geol.* **2014**, *352*, 451–468. [CrossRef]
9. Williamson, C.; Roshko, A. Vortex formation in the wake of an oscillating cylinder. *J. Fluids Struct.* **1988**, *2*, 355–381. [CrossRef]
10. Gabbai, R.; Benaroya, H. An overview of modeling and experiments of vortex-induced vibration of circular cylinders. *J. Sound Vib.* **2005**, *282*, 575–616. [CrossRef]
11. Zhao, M. A review of recent studies on the control of vortex-induced vibration of circular cylinders. *Ocean. Eng.* **2023**, *285*, 115389. [CrossRef]
12. Hong, K.S.; Shah, U.H. Vortex-induced vibrations and control of marine risers: A review. *Ocean. Eng.* **2018**, *152*, 300–315. [CrossRef]
13. Devenport, W.; Alexander, N.; Glegg, S.; Wang, M. The Sound of Flow Over Rigid Walls. *Annu. Rev. Fluid Mech.* **2018**, *50*, 435–458. [CrossRef]
14. Wang, M.; Freund, J.B.; Lele, S.K. Computational predictions of flow-induced sound. *Annu. Rev. Fluid Mech.* **2006**, *38*, 483–512. [CrossRef]
15. Moreau, S. The third golden age of aeroacoustics. *Phys. Fluids* **2022**, *34*, 031301. [CrossRef]
16. Zhao, F.; Hung, D.L. Applications of machine learning to the analysis of engine in-cylinder flow and thermal process: A review and outlook. *Appl. Therm. Eng.* **2023**, *220*, 119633. [CrossRef]
17. Krishan, G.; Aw, K.C.; Sharma, R.N. Synthetic jet impingement heat transfer enhancement–a review. *Appl. Therm. Eng.* **2019**, *149*, 1305–1323. [CrossRef]
18. Arshad, A.; Jabbal, M.; Yan, Y. Synthetic jet actuators for heat transfer enhancement—A critical review. *Int. J. Heat Mass Transf.* **2020**, *146*, 118815. [CrossRef]
19. Williamson, C.; Govardhan, R. Vortex-induced vibrations. *Annu. Rev. Fluid Mech.* **2004**, *36*, 413–455. [CrossRef]
20. Li, S.; Rival, D.E.; Wu, X. Sound source and pseudo-sound in the near field of a circular cylinder in subsonic conditions. *J. Fluid Mech.* **2021**, *919*, A43. [CrossRef]
21. Inoue, O.; Hatakeyama, N. Sound generation by a two-dimensional circular cylinder in a uniform flow. *J. Fluid Mech.* **2002**, *471*, 285–314. [CrossRef]
22. Collis, S.S.; Joslin, R.D.; Seifert, A.; Theofilis, V. Issues in active flow control: Theory, control, simulation, and experiment. *Progress Aerosp. Sci.* **2004**, *40*, 237–289. [CrossRef]
23. Oruç, V. Strategies for the applications of flow control downstream of a bluff body. *Flow Meas. Instrum.* **2017**, *53*, 204–214. [CrossRef]
24. Choi, H.; Jeon, W.P.; Kim, J. Control of Flow Over a Bluff Body. *Annu. Rev. Fluid Mech.* **2008**, *40*, 113–139. [CrossRef]
25. Kasagi, N.; Suzuki, Y.; Fukagata, K. Microelectromechanical Systems–Based Feedback Control of Turbulence for Skin Friction Reduction. *Annu. Rev. Fluid Mech.* **2009**, *41*, 231–251. [CrossRef]
26. Cattafesta, L.N.; Sheplak, M. Actuators for Active Flow Control. *Annu. Rev. Fluid Mech.* **2011**, *43*, 247–272. [CrossRef]
27. Dong, S.; Triantafyllou, G.S.; Karniadakis, G.E. Elimination of Vortex Streets in Bluff-Body Flows. *Phys. Rev. Lett.* **2008**, *100*, 204501. [CrossRef]
28. Abdolahipour, S.; Mani, M.; Taleghani, A.S. Parametric study of a frequency-modulated pulse jet by measurements of flow characteristics. *Phys. Scr.* **2021**, *96*, 125012. [CrossRef]
29. Abdolahipour, S.; Mani, M.; Shams Taleghani, A. Pressure Improvement on a Supercritical High-Lift Wing Using Simple and Modulated Pulse Jet Vortex Generator. *Flow Turbul. Combust.* **2022**, *109*, 65–100. [CrossRef]
30. Abdolahipour, S.; Mani, M.; Shams Taleghani, A. Experimental Investigation of Flow Control on a High-Lift Wing Using Modulated Pulse Jet Vortex Generator. *J. Aerosp. Eng.* **2022**, *35*, 05022001. [CrossRef]
31. Abdolahipour, S. Effects of low and high frequency actuation on aerodynamic performance of a supercritical airfoil. *Front. Mech. Eng.* **2023**, *9*, 1290074. [CrossRef]
32. Mirzaei, M.; Taleghani, A.S.; Shadaram, A. Experimental Study of Vortex Shedding Control Using Plasma Actuator. *Appl. Mech. Mater.* **2012**, *186*, 75–86. [CrossRef]
33. Brunton, S.L.; Noack, B.R. Closed-Loop Turbulence Control: Progress and Challenges. *Appl. Mech. Rev.* **2015**, *67*, 050801. [CrossRef]

34. Kim, J.; Bewley, T.R. A Linear Systems Approach to Flow Control. *Annu. Rev. Fluid Mech.* **2007**, *39*, 383–417. [CrossRef]
35. Rowley, C.W.; Dawson, S.T. Model Reduction for Flow Analysis and Control. *Annu. Rev. Fluid Mech.* **2017**, *49*, 387–417. [CrossRef]
36. Taira, K.; Hemati, M.S.; Brunton, S.L.; Sun, Y.; Duraisamy, K.; Bagheri, S.; Dawson, S.T.M.; Yeh, C.A. Modal Analysis of Fluid Flows: Applications and Outlook. *AIAA J.* **2020**, *58*, 998–1022. [CrossRef]
37. Brenner, M.P.; Eldredge, J.D.; Freund, J.B. Perspective on machine learning for advancing fluid mechanics. *Phys. Rev. Fluids* **2019**, *4*, 100501. [CrossRef]
38. Vinuesa, R. Perspectives on predicting and controlling turbulent flows through deep learning. *Phys. Fluids* **2024**, *36*, 031401. [CrossRef]
39. Brunton, S.L.; Noack, B.R.; Koumoutsakos, P. Machine learning for fluid mechanics. *Annu. Rev. Fluid Mech.* **2020**, *52*, 477–508. [CrossRef]
40. WU, Z.; FAN, D.W.; ZHOU, Y. Advances in control of turbulence by artificial intelligence: Systems, algorithms, achievements and data analysis methods. *Adv. Mech.* **2023**, *53*, 273.
41. Park, D.; Ladd, D.; Hendricks, E. Feedback control of von Kármán vortex shedding behind a circular cylinder at low Reynolds numbers. *Phys. Fluids* **1994**, *6*, 2390–2405. [CrossRef]
42. Zhang, M.; Cheng, L.; Zhou, Y. Closed-loop-controlled vortex shedding and vibration of a flexibly supported square cylinder under different schemes. *Phys. Fluids* **2004**, *16*, 1439–1448. [CrossRef]
43. Lu, L.; Qin, J.M.; Teng, B.; Li, Y.C. Numerical investigations of lift suppression by feedback rotary oscillation of circular cylinder at low Reynolds number. *Phys. Fluids* **2011**, *23*, 033601. [CrossRef]
44. Du, L.; Sun, X. Noise reduction by feedback rotary oscillation of a three-dimensional circular cylinder. *J. Fluids Struct.* **2019**, *84*, 421–439. [CrossRef]
45. Yun, J.; Lee, J. Active proportional feedback control of turbulent flow over a circular cylinder with averaged velocity sensor. *Phys. Fluids* **2022**, *34*, 095133. [CrossRef]
46. Wang, C.; Tang, H.; Yu, S.C.M.; Duan, F. Active control of vortex-induced vibrations of a circular cylinder using windward-suction-leeward-blowing actuation. *Phys. Fluids* **2016**, *28*, 053601. [CrossRef]
47. Vicente-Ludlam, D.; Barrero-Gil, A.; Velazquez, A. Flow-induced vibration control of a circular cylinder using rotational oscillation feedback. *J. Fluid Mech.* **2018**, *847*, 93–118. [CrossRef]
48. Song, J.; Du, J.; Gao, X. Applying PID control to 2-dof vortex induced vibration of a cylinder. *Ocean. Eng.* **2024**, *300*, 117295. [CrossRef]
49. Hasheminejad, S.M.; Rabiee, A.H.; Bahrami, H. Active closed-loop vortex-induced vibration control of an elastically mounted circular cylinder at low Reynolds number using feedback rotary oscillations. *Acta Mech.* **2018**, *229*, 231–250. [CrossRef]
50. Rabiee, A.H.; Esmaeili, M. Simultaneous vortex- and wake-induced vibration suppression of tandem-arranged circular cylinders using active feedback control system. *J. Sound Vib.* **2020**, *469*, 115131. [CrossRef]
51. Debien, A.; Von Krbek, K.A.; Mazellier, N.; Duriez, T.; Cordier, L.; Noack, B.R.; Abel, M.W.; Kourta, A. Closed-loop separation control over a sharp edge ramp using genetic programming. *Exp. Fluids* **2016**, *57*, 40. [CrossRef]
52. Li, R.; Noack, B.R.; Cordier, L.; Borée, J.; Harambat, F. Drag reduction of a car model by linear genetic programming control. *Exp. Fluids* **2017**, *58*, 103. [CrossRef]
53. Raibaudo, C.; Zhong, P.; Noack, B.R.; Martinuzzi, R.J. Machine learning strategies applied to the control of a fluidic pinball. *Phys. Fluids* **2020**, *32*, 015108. [CrossRef]
54. Raibaudo, C.; Martinuzzi, R.J. Unsteady actuation and feedback control of the experimental fluidic pinball using genetic programming. *Exp. Fluids* **2021**, *62*, 219. [CrossRef]
55. Ren, F.; Wang, C.; Tang, H. Active control of vortex-induced vibration of a circular cylinder using machine learning. *Phys. Fluids* **2019**, *31*, 093601. [CrossRef]
56. Castellanos, R.; Cornejo Maceda, G.Y.; de la Fuente, I.; Noack, B.R.; Ianiro, A.; Discetti, S. Machine-learning flow control with few sensor feedback and measurement noise. *Phys. Fluids* **2022**, *34*, 047118. [CrossRef]
57. Rabault, J.; Kuchta, M.; Jensen, A.; Réglade, U.; Cerardi, N. Artificial neural networks trained through deep reinforcement learning discover control strategies for active flow control. *J. Fluid Mech.* **2019**, *865*, 281–302. [CrossRef]
58. Ren, F.; Rabault, J.; Tang, H. Applying deep reinforcement learning to active flow control in weakly turbulent conditions. *Phys. Fluids* **2021**, *33*, 037121. [CrossRef]
59. Paris, R.; Beneddine, S.; Dandois, J. Robust flow control and optimal sensor placement using deep reinforcement learning. *J. Fluid Mech.* **2021**, *913*, A25. [CrossRef]
60. Li, J.; Zhang, M. Reinforcement-learning-based control of confined cylinder wakes with stability analyses. *J. Fluid Mech.* **2022**, *932*, A44. [CrossRef]
61. Varela, P.; Suárez, P.; Alcántara-Ávila, F.; Miró, A.; Rabault, J.; Font, B.; García-Cuevas, L.M.; Lehmkuhl, O.; Vinuesa, R. Deep Reinforcement Learning for Flow Control Exploits Different Physics for Increasing Reynolds Number Regimes. *Actuators* **2022**, *11*, 359. [CrossRef]
62. Zhao, F.; Zhou, Y.; Ren, F.; Tang, H.; Wang, Z. Mitigating the lift of a circular cylinder in wake flow using deep reinforcement learning guided self-rotation. *Ocean. Eng.* **2024**, *306*, 118138. [CrossRef]
63. Wang, Q.; Yan, L.; Hu, G.; Chen, W.; Rabault, J.; Noack, B.R. Dynamic feature-based deep reinforcement learning for flow control of circular cylinder with sparse surface pressure sensing. *J. Fluid Mech.* **2024**, *988*, A4. [CrossRef]

64. Ren, F.; Du, J.; Li, G. Intelligent self-adaptive control for mitigating lift fluctuations of a circular cylinder. *Chin. J. Theor. Appl. Mech.* **2024**, *56*, 972–979. [CrossRef]
65. Chen, J.; Chen, S.; Ren, F.; Hu, H. Artificiallyintelligent control of drag reduction around a circular cylinder based on wall pressure feedback. *Acta Phys. Sin.* **2022**, *71*, 084701-1. [CrossRef]
66. Ren, F.; Wang, C.; Tang, H. Bluff body uses deep reinforcement learning trained active flow control to achieve hydrodynamic stealth. *Phys. Fluids* **2021**, *33*, 093602. [CrossRef]
67. Fan, D.; Yang, L.; Wang, Z.; Triantafyllou, M.S.; Karniadakis, G.E. Reinforcement learning for bluff body active flow control in experiments and simulations. *Proc. Natl. Acad. Sci.* **2020**, *117*, 26091–26098. [CrossRef]
68. Wang, Z.; Fan, D.; Jiang, X.; Triantafyllou, M.S.; Karniadakis, G.E. Deep reinforcement transfer learning of active control for bluff body flows at high Reynolds number. *J. Fluid Mech.* **2023**, *973*, A32. [CrossRef]
69. Zheng, C.; Ji, T.; Xie, F.; Zhang, X.; Zheng, H.; Zheng, Y. From active learning to deep reinforcement learning: Intelligent active flow control in suppressing vortex-induced vibration. *Phys. Fluids* **2021**, *33*, 063607. [CrossRef]
70. Ren, F. Intelligent flow control for vortex-induced vibration of cylinder. *Chin. J. Hydrodyn.* **2022**, *37*, 757–762. [CrossRef]
71. Chen, W.; Wang, Q.; Yan, L.; Hu, G.; Noack, B.R. Deep reinforcement learning-based active flow control of vortex-induced vibration of a square cylinder. *Phys. Fluids* **2023**, *35*, 053610. [CrossRef]
72. Ren, F.; Wang, C.; Song, J.; Tang, H. Deep reinforcement learning finds a new strategy for vortex-induced vibration control. *J. Fluid Mech.* **2024**, *990*, A7. [CrossRef]
73. Mei, Y.F.; Zheng, C.; Aubry, N.; Li, M.G.; Wu, W.T.; Liu, X. Active control for enhancing vortex induced vibration of a circular cylinder based on deep reinforcement learning. *Phys. Fluids* **2021**, *33*, 103604. [CrossRef]
74. Ren, F.; Zhang, F.; Zhu, Y.; Wang, Z.; Zhao, F. Enhancing heat transfer from a circular cylinder undergoing vortex induced vibration based on reinforcement learning. *Appl. Therm. Eng.* **2024**, *236*, 121919. [CrossRef]
75. Zheng, C.; Xie, F.; Ji, T.; Zhang, X.; Lu, Y.; Zhou, H.; Zheng, Y. Data-efficient deep reinforcement learning with expert demonstration for active flow control. *Phys. Fluids* **2022**, *34*, 113603. [CrossRef]
76. Nair, A.G.; Yeh, C.A.; Kaiser, E.; Noack, B.R.; Brunton, S.L.; Taira, K. Cluster-based feedback control of turbulent post-stall separated flows. *J. Fluid Mech.* **2019**, *875*, 345–375. [CrossRef]
77. Wang, X.; Deng, N.; Cornejo Maceda, G.Y.; Noack, B.R. Cluster-based control for net drag reduction of the fluidic pinball. *Phys. Fluids* **2023**, *35*, 023601. [CrossRef]
78. Curle, N. The Influence of Solid Boundaries Upon Aerodynamic Sound. *Proc. R. Soc. A* **1955**, *231*, 505–514.
79. Rabault, J.; Ren, F.; Zhang, W.; Tang, H.; Xu, H. Deep reinforcement learning in fluid mechanics: A promising method for both active flow control and shape optimization. *J. Hydrodyn.* **2020**, *32*, 234–246. [CrossRef]
80. Ren, F.; Hu, H.B.; Tang, H. Active flow control using machine learning: A brief review. *J. Hydrodyn.* **2020**, *32*, 247–253. [CrossRef]
81. Ren, F.; Gao, C.; Tang, H. Machine learning for flow control: Applications and development trends. *Acta Aeronaut. Astronaut. Sin.* **2021**, *42*, 524686.
82. Gautier, N.; Aider, J.L.; Duriez, T.; Noack, B.; Segond, M.; Abel, M. Closed-loop separation control using machine learning. *J. Fluid Mech.* **2015**, *770*, 442–457. [CrossRef]
83. Ren, F.; Song, B.; Zhang, Y.; Hu, H. A GPU-accelerated solver for turbulent flow and scalar transport based on the Lattice Boltzmann method. *Comput. Fluids* **2018**, *173*, 29–36. [CrossRef]
84. Ren, F.; Song, B.; Hu, H. Lattice Boltzmann simulations of turbulent channel flow and heat transport by incorporating the Vreman model. *Appl. Therm. Eng.* **2018**, *129*, 463–471. [CrossRef]
85. Kaelbling, L.P.; Littman, M.L.; Moore, A.W. Reinforcement learning: A survey. *J. Artif. Intell. Res.* **1996**, *4*, 237–285. [CrossRef]
86. Silver, D.; Schrittwieser, J.; Simonyan, K.; Antonoglou, I.; Hassabis, D. Mastering the game of Go without human knowledge. *Nature* **2017**, *550*, 354–359. [CrossRef]
87. Silver, D.; Huang, A.; Maddison, C.J.; Guez, A.; Sifre, L.; Driessche, G.V.D.; Schrittwieser, J.; Antonoglou, I.; Panneershelvam, V.; Lanctot, M. Mastering the game of Go with deep neural networks and tree search. *Nature* **2016**, *529*, 484–489. [CrossRef]
88. Reddy, G.; Celani, A.; Sejnowski, T.J.; Vergassola, M. Learning to soar in turbulent environments. *Proc. Natl. Acad. Sci. USA* **2016**, *113*, E4877. [CrossRef]
89. Verma, S.; Novati, G.; Koumoutsakos, P. Efficient collective swimming by harnessing vortices through deep reinforcement learning. *Proc. Natl. Acad. Sci. USA* **2018**, *115*, 5849–5854. [CrossRef]
90. Vignon, C.; Rabault, J.; Vinuesa, R. Recent advances in applying deep reinforcement learning for flow control: Perspectives and future directions. *Phys. Fluids* **2023**, *35*, 031301. [CrossRef]
91. Xie, F.; Zheng, C.; Ji, T.; Zhang, X.; Bi, R.; Zhou, H.; Zheng, Y. Deep Reinforcement Learning: A New Beacon for Intelligent Active Flow Control. *Aerosp. Res. Commun.* **2023**, *1*, 11130. [CrossRef]
92. Belus, V.; Rabault, J.; Viquerat, J.; Che, Z.; Hachem, E.; Reglade, U. Exploiting locality and translational invariance to design effective deep reinforcement learning control of the 1-dimensional unstable falling liquid film. *AIP Adv.* **2019**, *9*, 125014. [CrossRef]
93. Schulman, J.; Wolski, F.; Dhariwal, P.; Radford, A.; Klimov, O. Proximal policy optimization algorithms. *arXiv* **2017**, arXiv:1707.06347.
94. Wang, Q.; Yan, L.; Hu, G.; Li, C.; Xiao, Y.; Xiong, H.; Rabault, J.; Noack, B.R. DRLinFluids: An open-source Python platform of coupling deep reinforcement learning and OpenFOAM. *Phys. Fluids* **2022**, *34*, 081801. [CrossRef]
95. Mao, Y.; Zhong, S.; Yin, H. DRLFluent: A distributed co-simulation framework coupling deep reinforcement learning with Ansys-Fluent on high-performance computing systems. *J. Comput. Sci.* **2023**, *74*, 102171. [CrossRef]

96. Song, J.; Zhang, F.; Zhao, Y.; Ren, F.; Hu, H. Direct simulations of external flow and noise radiation using the generalized interpolation-supplemented cascaded lattice Boltzmann method. *Comput. Fluids* **2024**, *280*, 106347. [CrossRef]
97. Song, J.; Hu, H.; Li, G.; Zhang, H.; Ren, F. Generalized interpolation-supplemented cascaded lattice Boltzmann method for noise radiated from a circular cylinder. *J. Comput. Phys.* **2024**, *517*, 113319. [CrossRef]
98. Rabault, J.; Kuhnle, A. Accelerating deep reinforcement learning strategies of flow control through a multi-environment approach. *Phys. Fluids* **2019**, *31*, 094105. [CrossRef]
99. Pino, F.; Schena, L.; Rabault, J.; Mendez, M.A. Comparative analysis of machine learning methods for active flow control. *J. Fluid Mech.* **2023**, *958*, A39. [CrossRef]
100. Hou, C.; Deng, N.; Noack, B.R. Trajectory-optimized cluster-based network model for the sphere wake. *Phys. Fluids* **2022**, *34*, 085110. [CrossRef]